JOURNAL OF THERMOPHYSICS AND HEAT TRANSFER
Vol. 19, No. 4, October–December 2005

Technical Notes

TECHNICAL NOTES are short manuscripts describing new developments or important results of a preliminary nature. These Notes should not exceed 2500 words (where a figure or table counts as 200 words). Following informal review by the Editors, they may be published within a few months of the date of receipt. Style requirements are the same as for regular contributions (see inside back cover).

Numerically Stabilizing Ill-Posed Moving Surface Problems Through Heat-Rate Sensors

J. I. Frankel*
University of Tennessee, Knoxville, Tennessee 37996-2210
and
John L. Lawless†
Redwood Scientific, Inc., Pacifica, California 94044-4300

Nomenclature

B_M^2	=	deterministic bias, Eq. (10c)
b	=	constant in Gaussian function, s, Eq. (7)
c_p	=	heat capacity, kJ/(kg°C)
$I_j(z)$	=	jth modified Bessel function
K	=	convolution kernel, Eq. (1c)
k	=	thermal conductivity, W/(m°C)
M	=	number of data points
M_a	=	convolution kernel, Eq. (5a)
M_b	=	convolution kernel, Eq. (5b)
N	=	convolution kernel, Eq. (6b)
q''	=	dimensional heat flux, W/m^2
q_s''	=	surface heat flux, W/m^2
q_0''	=	maximum Gaussian heat-flux value, W/m^2
T	=	temperature, °C
T_i	=	discrete temperature, °C
T_s	=	surface temperature, °C
T_0	=	initial temperature, °C
t	=	time, s
$t_{\max}$	=	maximum time, s
t_0	=	dummy variable, s
u	=	velocity of moving surface, m/s
v	=	dummy variable, Eq. (3)
x	=	spatial variable, m
z	=	dummy argument
α	=	thermal diffusivity, m^2/s
β	=	constant, Eq. (1c)
ϵ_i	=	noise factor, Eqs. (8a) and (8b)
θ	=	temperature difference, $T_s - T_0$, °C
λ	=	constant, Eq. (1c)
ρ	=	density, kg/m^3
σ	=	constant, Eq. (7)
σ_M^2	=	variance, Eq. (10d)

Received 23 May 2004; revision received 5 January 2005; accepted for publication 5 January 2005.

*Professor, Mechanical, Aerospace and Biomedical Engineering Department; vfrankel@earthlink.net. Senior Member AIAA.
†President; lawless@alumni.princeton.edu. Senior Member AIAA.

Introduction

PREVIOUS work[1–3] has shown that heat-transfer problems previously thought to be ill posed can become well posed if different sensors are chosen to provide the initial and/or boundary conditions. In particular, relative to conventional temperature T or heat-flux q'' sensors, there is a strong advantage to sensors that directly measure time-derivative data, such as $\mathrm{d}T/\mathrm{d}t$, $\mathrm{d}q''/\mathrm{d}t$, etc. In an effort to define the requirements for such sensors as well as to demonstrate their potential uses, numerical solutions of a heat-transfer problem are presented herein. Solutions are performed using simulated data from a temperature sensor and using simulated data from a $\mathrm{d}T/\mathrm{d}t$ sensor. The performance of these sensors in the presence of noise and increasing sample rates is compared. The results demonstrate that, for the accuracy of the computed results, the choice of data space, T or $\mathrm{d}T/\mathrm{d}t$ in this case, can be far more important than the accuracy of the sensor.

Kulish and Novozhilov[4] recently developed an integral relationship between the local temperature and heat flux in a semi-infinite domain with a constant velocity moving boundary. The half-space is initially at the uniform temperature $T(x, 0) = T_0$ while moving at constant velocity u. At $t = 0$, the surface at $x = 0$ is subjected to a heat flux denoted as $q_s''(t)$. Here, T is the temperature, $x \geq 0, t \geq 0$ are the spatial and temporal domains. Penner and Olfe[5] also describe such problems with inclusion of volumetric radiative effects.

Kulish and his colleagues[4,6–8] have investigated several transient, linear, half-space heat-transfer problems and developed novel integral relationships between the temperature and heat flux. This local relationship (not solution) is quite useful in the half-space investigations considered by Kulish and his colleagues. Their integral relationships permit two distinct interpretations. The first is direct and stable while the second is inverse and normally unstable (depending on the data space). The first involves the specification of the local heat flux from which the local temperature is determined. This statement only requires the implementation of integration. The second involves the specification of temperature from which the local heat flux is reconstructed. This situation leads to a Volterra integral equation of the first kind. If discrete, noisy temperature data are specified, then this formulation is unstable.

The heat flux[4,6–8] is analytically provided, leading to a relatively simple numerical procedure for obtaining the corresponding temperature. Frankel et al.[1] have noted that this defines a stable numerical direction. However, determining the heat flux from discrete, noisy temperature data leads to an unstable numerical prediction. That is, the prediction noticeably worsens as either the noise level or sample density increases. Regularization methods are normally implemented in order to arrive at an acceptable prediction. Determining the optimal regularization parameter is crucial and often difficult to achieve. The quality of the prediction is closely connected to the regularization parameter. To date, no steadfast rigorous mathematical rules are available. To circumvent this unfavorable characteristic, Frankel and his colleagues[1–3] have analyzed the concept of using an alternative data space. This idea involves using higher time-derivative measurements involving the temperature and heat flux. The mechanical analogy (displacement → velocity → acceleration) is quite apparent. Frankel and his colleagues[1–3] have developed several theoretical concepts for measuring the proposed hierarchical[1] system involving $\mathrm{d}T/\mathrm{d}t$, $\mathrm{d}q''/\mathrm{d}t$, and $\mathrm{d}^2T/\mathrm{d}t^2$.

The move toward real-time analysis can benefit from the development of such higher-time-derivative measurement techniques. For example, the health management of machines subjected to high thermal stresses might require the inferences of both temperature and heat fluxes in order to devise a cooling strategy. The numerical solutions presented herein describe how both quantities on a surface can be reliably inferred from a single dT/dt sensor. More complex health management problems might require other combinations of sensors and analysis, but the choice of sensor data space is expected to remain important.

Mathematical Formulation

The linear, heat-conduction equation under consideration is given by[4]

$$\frac{\partial T}{\partial t}(x,t) + u\frac{\partial T}{\partial x}(x,t) = \alpha\frac{\partial^2 T}{\partial x^2}(x,t) \qquad x,t \geq 0 \tag{1a}$$

where α is the thermal diffusivity and u is the speed of the domain boundary[5] moving from right to left in order for the ablating surface to remain at $x=0$ (i.e., $u \leq 0$). Kulish and Novozhilov[4] develop an integral relationship between the temperature and heat flux as

$$T(x,t) = T_0 + \int_{t_0=0}^{t} q''(x,t_0)K(t-t_0)\,dt_0 \qquad x,t \geq 0 \tag{1b}$$

with the convolution kernel $K(t-t_0)$ given as

$$K(t-t_0) = \frac{\lambda e^{-u^2(t-t_0)/4\alpha}}{\sqrt{t-t_0}} + \beta erfc\left(-\frac{u}{2}\sqrt{\frac{t-t_0}{\alpha}}\right) \qquad t > t_0 \tag{1c}$$

where $\lambda = 1/\sqrt{(\pi k\rho c_p)}$, $\beta = u/(2k)$, and $erfc(z)$ is the complementary error function (Ref. 9, p. 297) with argument z. At the surface ($x=0$), Eq. (1b) reduces to

$$T_s(t) = T_0 + \int_{t_0=0}^{t} q_s''(t_0)K(t-t_0)\,dt_0 \qquad t \geq 0 \tag{1d}$$

where $T_s(t) = T(0,t)$ and $q_s''(t) = q''(0,t)$. Under the condition of no motion ($u=0$), Eq. (1b) reduces to

$$T(x,t) = T_0 + \lambda\int_{t_0=0}^{t} \frac{q''(x,t_0)}{\sqrt{t-t_0}}\,dt_0 \qquad x,t \geq 0 \tag{1e}$$

The Green's function solution[1] leads to the identical result at the boundary $x=0$. A significant amount of literature[1,3,10–12] exists using Eq. (1e) at $x=0$. For example, some arcjet studies make use of Eq. (1e) at $x=0$ for estimating the heat flux based on surface-temperature measurements. This leads to unstable numerical results requiring additional postprocessing and thus removes any real-time interpretation.

An elegant manner[4] for confirming the integral relation is available with the aid of the equivalent heat-flux formulation of the heat equation, namely,

$$\frac{\partial q''}{\partial t}(x,t) + u\frac{\partial q''}{\partial x}(x,t) = \alpha\frac{\partial^2 q''}{\partial x^2}(x,t) \qquad x,t \geq 0 \tag{2}$$

That is, one can verify Eq. (1b) through comparison with Eq. (2) upon substituting Eq. (1b) into Eq. (1a) and making use of fundamental calculus.

Deriving a Stabilized Data Set: Future Sensors

As $u \to 0$ in Eq. (1d), the classical Abel integral equation results having known inversion properties.[1,13–16] Frankel et al.[1] developed a hierarchical inversion sequence of the Abel equation to provide insight into devising a proper sensor sequence for stable predictions. That is, an Abel inversion[1] indicates a stable data space from which data should be collected. For simplicity but without loss of generality, the boundary relationship at $x=0$ is the focus of the present analysis, though any position x can be equally analyzed using the approach taken here. Also, for simplicity, let $\theta(t) = T(0,t) - T_0 = T_s(t) - T_0$, where $T_0 = 0°C$. The Abel inversion begins by letting $t \to v$ in Eq. (1d), operating on the result with $dv/\sqrt{(t-v)}$ and then integrating over the domain of interest to formally arrive at

$$\int_{v=0}^{t} \frac{\theta(v)}{\sqrt{t-v}}\,dv = \int_{v=0}^{t} \frac{1}{\sqrt{t-v}}\int_{t_0=0}^{v} q_s''(t_0)K(v-t_0)\,dt_0\,dv \qquad t \geq 0 \tag{3}$$

Carefully interchanging orders of integration on the double integral and then renaming the dummy variable in the left-hand side for convenience produces

$$\int_{t_0=0}^{t} \frac{\theta(t_0)}{\sqrt{t-t_0}}\,dt_0 = \lambda\int_{t_0=0}^{t} q_s''(t_0)M_a(t-t_0)\,dt_0 + \beta\int_{t_0=0}^{t} q_s''(t_0)M_b(t-t_0)\,dt_0 \tag{4}$$

where the convolution kernels $M_a(t-t_0)$ and $M_b(t-t_0)$ are defined as and integrate to

$$M_a(t-t_0) = \int_{v=t_0}^{t} \frac{e^{-u^2(v-t_0)/4\alpha}}{\sqrt{v-t_0}\sqrt{t-v}}\,dv = \pi e^{-u^2(t-t_0)/8\alpha} I_0\left[\frac{u^2(t-t_0)}{8\alpha}\right] \tag{5a}$$

$$M_b(t-t_0) = \int_{v=t_0}^{t} \frac{erfc\left(-u\sqrt{v-t_0}\big/2\sqrt{\alpha}\right)}{\sqrt{t-v}}\,dv = 2\sqrt{t-t_0} + u\sqrt{\frac{\pi}{4\alpha}}e^{-u^2(t-t_0)/8\alpha}(t-t_0) \times \left\{I_0\left[\frac{u^2(t-t_0)}{8\alpha}\right] + I_1\left[\frac{u^2(t-t_0)}{8\alpha}\right]\right\} \qquad t > t_0 \tag{5b}$$

where $I_p(z)$ is the pth modified Bessel function (Ref. 9, p. 374) having argument z. Next, integrate the left-hand side of Eq. (4) by parts and then operate on Eq. (4) with d/dt. Making use of Leibnitz's rule (Ref. 17, p. 287) on this result and finally returning to the original dependent variable yields

$$\int_{t_0=0}^{t} \frac{dT_s(t_0)}{dt_0}\frac{dt_0}{\sqrt{t-t_0}} = \lambda\pi q_s''(t) + \int_{t_0=0}^{t} q_s''(t_0)N(t-t_0)\,dt_0 \qquad t \geq 0 \tag{6a}$$

where the convolution kernel $N(t-t_0)$ is defined as

$$N(t-t_0) = \lambda\frac{\partial M_a}{\partial t}(t-t_0) + \beta\frac{\partial M_b}{\partial t}(t-t_0) \qquad t > t_0 \tag{6b}$$

with

$$\frac{\partial M_a}{\partial t}(t-t_0) = \frac{\pi u^2}{8\alpha}e^{-u^2(t-t_0)/8\alpha} \times \left\{I_1\left[\frac{u^2(t-t_0)}{8\alpha}\right] - I_0\left[\frac{u^2(t-t_0)}{8\alpha}\right]\right\} \tag{6c}$$

$$\frac{\partial M_b}{\partial t}(t-t_0) = \frac{1}{\sqrt{t-t_0}} + u\sqrt{\frac{\pi}{4\alpha}}e^{-u^2(t-t_0)/8\alpha} \times \left(I_0\left[\frac{u^2(t-t_0)}{8\alpha}\right] + I_1\left[\frac{u^2(t-t_0)}{8\alpha}\right] + \frac{u^2(t-t_0)}{16\alpha}\left\{-I_0\left[\frac{u^2(t-t_0)}{8\alpha}\right] + I_2\left[\frac{u^2(t-t_0)}{8\alpha}\right]\right\}\right) \qquad t > t_0 \tag{6d}$$

Equation (6a) is a weakly singular Volterra integral equation of the second kind[13–16] for $q_s''(t)$ when provided $\mathrm{d}T_s/\mathrm{d}t$. This is in stark contrast to Eq. (1d), which is a weakly singular Volterra integral equation of the first kind when provided T data. It is well known that first-kind Volterra equations[18,19] are mildly ill posed while second-kind Volterra equations are well posed. The weak singularity does not cause any difficulty because product integration rules[14] or singularity subtraction[16] can be used. Also, when $u = 0$ Eq. (6a) reduces to the well-known result[6]

$$q_s''(t) = \frac{1}{\lambda\pi}\int_{t_0=0}^{t} \frac{\mathrm{d}T_s(t_0)}{\mathrm{d}t_0}\frac{\mathrm{d}t_0}{\sqrt{t-t_0}} \qquad t \geq 0 \tag{6e}$$

The next section displays numerical results for a test case involving random error in the data spaces. It is assumed that other forms of error, such as bias, are accounted through calibration.

Because experimental data are inexact, its real-time use in numerical schemes must be viewed with some care. That is, real-time use requires using the interpreted value without consideration to its error band. This, of course, is incorrect but convenient. Differentiation of such data is well known to be ill posed in the classical sense.[20–22] It is not normally recommended to use these data exactly because they place too much emphasis on their inexact value. However, by changing the data space it will be demonstrated that measurements with a high degree of error can produce more accurate and stable results than measurements having a low degree of error. The choice of the data space must thus be considered. These remarks involve the direct measurement or interpretation of thermal "rate" quantities.

Numerical Predictions

Let us demonstrate several key issues by considering the heat flux of the Gaussian form[4]

$$q_s''(t) = q_0''e^{-[(t-b)/\sigma]^2} \qquad t \geq 0 \tag{7}$$

where q_0'' is the maximum heat-flux value acquired at $t = b$. The physical meanings for the parameters b and σ are self-evident. For the present study, inexact, discrete data for the surface temperature $\{T_{s,i}\}_{i=1}^{M}$ and surface heating/cooling rate $\{\mathrm{d}T_{s,i}/\mathrm{d}t\}_{i=1}^{M}$ are provided. Though not necessary, exact initial conditions are imposed at $t = 0$ owing to their availability. Again, for demonstration purposes the analysis and numerical results consider the surface at $x = 0$. This is not necessary as already noted. Kulish and Novozhilov[4] present temperature results when provided the exact, analytic heat-flux function. The physics of constant velocity motion u on the resulting surface temperature when provided the heat flux is well documented.[4] This study focuses on comparing two, discrete data forms (temperature T_s and heating/cooling rate $\mathrm{d}T_s/\mathrm{d}t$) and their abilities to predict the surface heat flux as the noise levels and sampling rates are varied.

Numerically exact temperature data are generated by discretizing Eq. (1d) using $q_s''(t)$ as defined in Eq. (7). Numerous numerical methods[15] are available for implementation. For this study, a product trapezoidal rule[14,15] is implemented for obtaining the discrete exact values of $T_s(t_i)$. A simple forward finite difference method is used to then develop the exact heating/cooling rate data set $\{\mathrm{d}T_s(t_i)/\mathrm{d}t\}_{i=0}^{M}$ based on these values. The noisy data sets can be developed based on locality with the aid of

$$T_{s,i} = T_s(t_i)(1 + \epsilon_1 Random_{1,i}[-1, 1]) \tag{8a}$$

$$\frac{\mathrm{d}T_{s,i}}{\mathrm{d}t} = \frac{\mathrm{d}T_s}{\mathrm{d}t}(t_i)(1 + \epsilon_2 Random_{2,i}[-1, 1]) \qquad i = 1, 2, \ldots, M \tag{8b}$$

or based on globality through

$$T_{s,i} = T_s(t_i) + \|T_s(t)\|_\infty \epsilon_1 Random_{1,i}[-1, 1] \tag{8c}$$

$$\frac{\mathrm{d}T_{s,i}}{\mathrm{d}t} = \frac{\mathrm{d}T_s}{\mathrm{d}t}(t_i) + \left\|\frac{\mathrm{d}T_s}{\mathrm{d}t}(t)\right\|_\infty \epsilon_2 Random_{2,i}[-1, 1] \qquad i = 1, 2, \ldots, M \tag{8d}$$

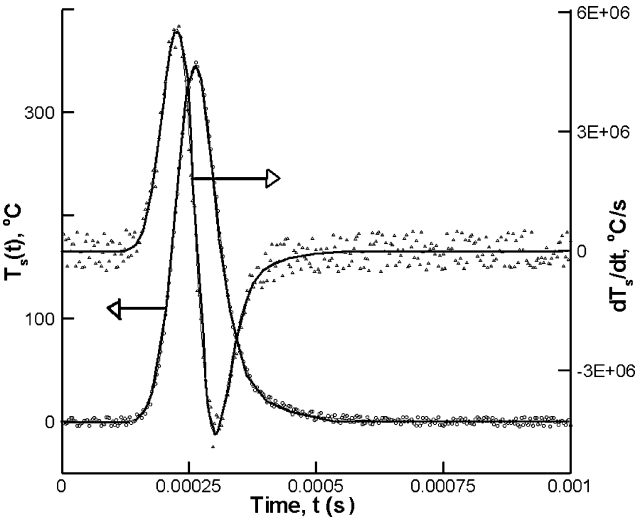

Fig. 1 Temperature $T_s(t)$ [——, exact; open discrete symbol, noisy data, $\epsilon_1 = 0.0125$, Eq. (8c)] and heating/cooling rate $\mathrm{d}T_s/\mathrm{d}t$ [——, exact; open discrete symbol, noisy data, $\epsilon_2 = 0.1$, Eq. (8d)] used for simulation when $M = 300$.

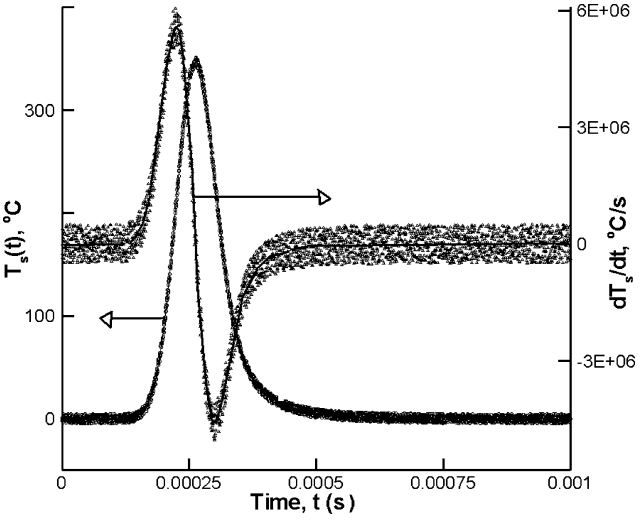

Fig. 2 Temperature $T_s(t)$ [——, exact; open discrete symbol, noisy data, $\epsilon_1 = 0.0125$, Eq. (8c)] and heating/cooling rate $\mathrm{d}T_s/\mathrm{d}t$ [——, exact; open discrete symbol, noisy data, $\epsilon_2 = 0.1$, Eq. (8d)] used for simulation when $M = 3000$.

where $\|\Psi\|_\infty = \max_{t\in[0,t_{\max}]}|\Psi(t)|$ is the infinity norm of the function $\Psi(t)$, $\epsilon_k, k = 1, 2$ are noise levels while $Random_{k,i}$ are randomly drawn numbers from a uniform distribution in the interval $[-1, 1]$ such that the mean error for each data set is zero. Both forms of data generation were tested. The global definitions given in Eqs. (8c) and (8d) are used in this study. The results associated with local error generation, as shown in Eqs. (8a) and (8b), works equally as well for verifying the hypothesis of this Note.

Figures 1 ($M = 300$) and 2 ($M = 3000$) display both the numerically exact solution and noisy data sets for the surface temperature $T_s(t)$ and heating/cooling rate $\mathrm{d}T_s/\mathrm{d}t$ when $\epsilon_1 = 0.0125$, $\epsilon_2 = 0.1$. Additionally, it is assumed that $u = -1$ m/s, $b = 2.5 \times 10^{-4}$ s, $\sigma = 5 \times 10^{-5}$ s, $q_0'' = 75$ kW/cm^2, $k = 52$ W/(m°C), and $\rho c_p = 1.73 \times 10^6$ J/(m^3°C). For these plots, the discrete time t_i is defined using $t_i = i\Delta t$, $i = 1, 2, \ldots, M$, where $\Delta t = t_{\max}/M$ and $t_{\max} = 0.001$ s. Throughout this presentation, solid lines represent numerically exact results, and open symbols represent discrete data. For this Note, only graphical results are presented for the velocity $u = -1$ m/s.

The relative simplicity of Eq. (1d) permits use of a hybrid product and Newton–Cotes right-hand rectangular rule. This simple numerical approach can be modified at a later time if required for

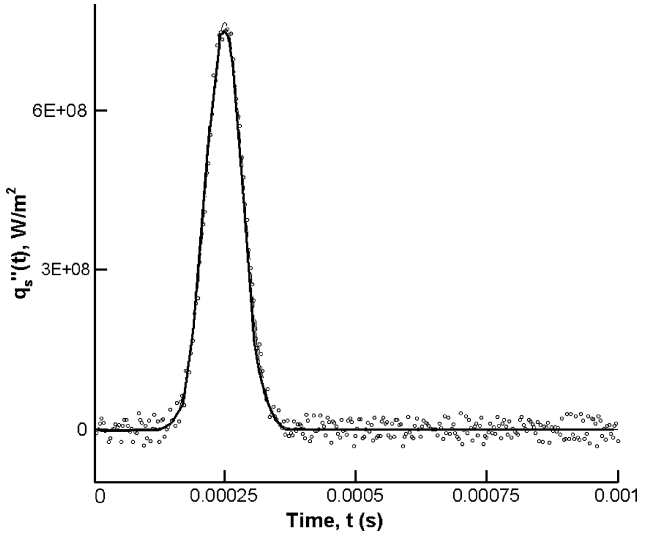

Fig. 3 Predicted heat fluxes $q_s''(t)$: a) ——, exact, Eq. (7); b) – – –, errorless data predictions, $\epsilon_1 = 0$, Eq. (1d); and c) open discrete symbol, noisy data predictions, $\epsilon_1 = 0.0125$, Eq. (1d) when $M = 300$.

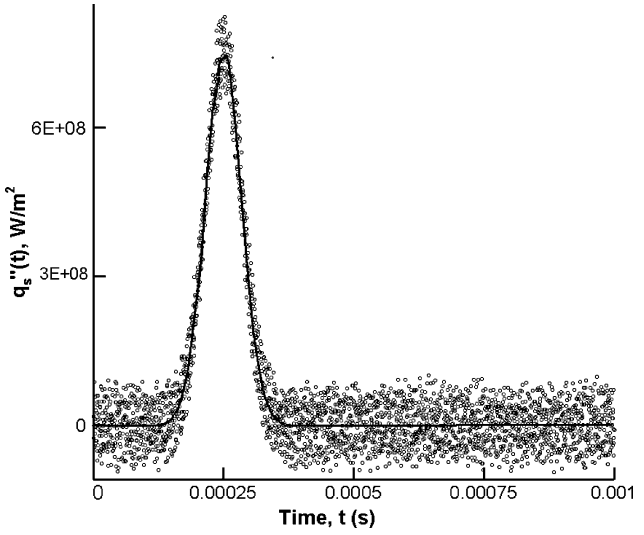

Fig. 5 Predicted heat fluxes $q_s''(t)$: a) ——, exact, Eq. (7); b) – – –, errorless data predictions, $\epsilon_1 = 0$, Eq. (1d); and c) open discrete symbol, noisy data predictions, $\epsilon_1 = 0.0125$, Eq. (1d) when $M = 3000$.

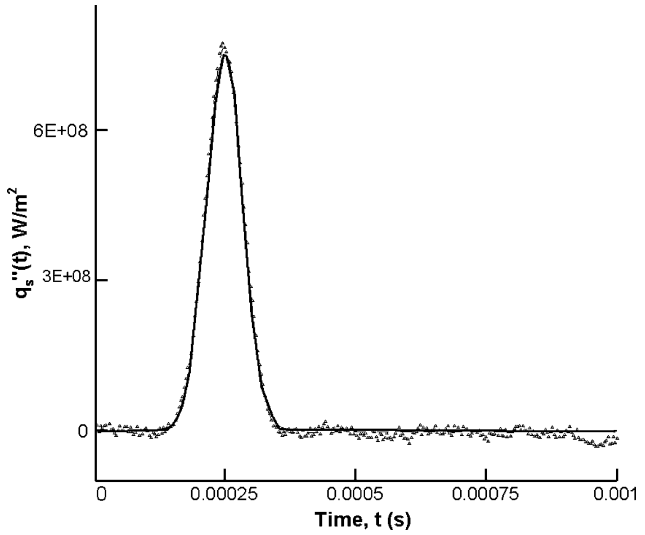

Fig. 4 Predicted heat fluxes $q_s''(t)$: a) ——, exact, Eq. (7); b) – – –, errorless data predictions, $\epsilon_2 = 0$, Eq. (6a); and c) open discrete symbol, noisy data predictions, $\epsilon_2 = 0.1$, Eq. (6a) when $M = 300$.

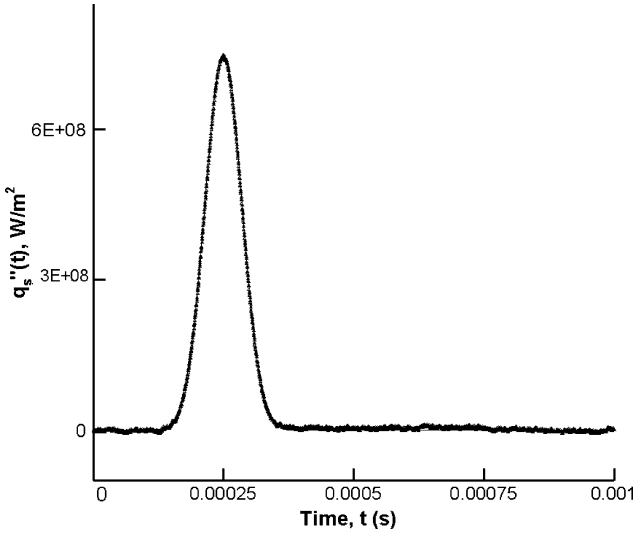

Fig. 6 Predicted heat fluxes $q_s''(t)$: a) ——, exact, Eq. (7); b) – – –, errorless data predictions, $\epsilon_2 = 0$, Eq. (6a); and c) open discrete symbol, noisy data predictions, $\epsilon_2 = 0.1$, Eq. (6a) when $M = 3000$.

defining a consistent numerical scheme. This implementation is also used for discretizing Eq. (6a). The product integration method is applied only to the singular kernel contributions while a conventional Newton–Cotes rectangular method is implemented elsewhere. Figures 3 and 4 present predictions for the surface heat flux based on the data presented in Fig. 1. Figure 3 displays 1) the exact heat flux given in Eq. (7) by the solid line, 2) the numerically predicted heat flux using Eq. (1b) when $\epsilon_1 = 0$ by the dashed line, and 3) the numerically predicted heat flux using Eq. (1b) when $\epsilon_1 = 0.0125$ by the open circles. The numerical method nearly replicates the exact heat flux when the discrete data contain no induced errors ($\epsilon_1 = 0$), that is, the solid and dashed lines are nearly indistinguishable. This indicates that the numerical method is functionally well. However, the poor convergence of the results with the noisy data indicate that the sample set size is insufficient for convergence.

Figure 4 presents a set of results corresponding to that of Fig. 3 with the exception that Eq. (6a) is resolved using heating/cooling rate data presented in Fig. 1. Figure 4 displays 1) the exact heat flux given in Eq. (7) by the solid line, 2) the numerically predicted heat flux using Eq. (6a) when $\epsilon_2 = 0$ by the dashed line, and 3) the numerically predicted heat flux using Eq. (6a) when $\epsilon_2 = 0.1$ by the open triangles. Again, as expected, the numerical procedure nearly emulates the exact solution when the discrete data contain zero noise. The noisy data set associated with the heating/cooling rate data produces a more accurate heat-flux prediction than the data developed by the corresponding temperature set containing less error. Error amplification is not graphically observed when using $\{dT_{s,i}/dt\}_{i=1}^{M}$. This is expected because Eq. (6a) is a second-kind Volterra equation. Solving Volterra equations are analogous to solving initial-value differential equations in that a marching method can be used. This permits near, real-time analysis to be performed.

Another annoying feature of ill-conditioned (or ill-posed) problems is observable as the approximation is refined or the sampling rate is increased. In direct or forward problems, normally better results are generated as the approximation is refined. This is not the case with ill-posed problems. As the approximation is refined, the error in the output can begin to increase. Thus, an optimal prediction occurs at some unknown juncture. Figures 5 and 6 present the predicted surface heat flux based on the data presented in Fig. 2. In these cases, the sample density is increased by a factor of 10 from $M = 300$ to 3000. Figure 5 displays the similar sets of results presented in Fig. 3, that is, 1) exact; 2) estimated using errorless data, $\epsilon_1 = 0$; and 3) predicted using noisy data, $\epsilon_1 = 0.0125$. It is evident that error amplification in the prediction occurs for fixed induced

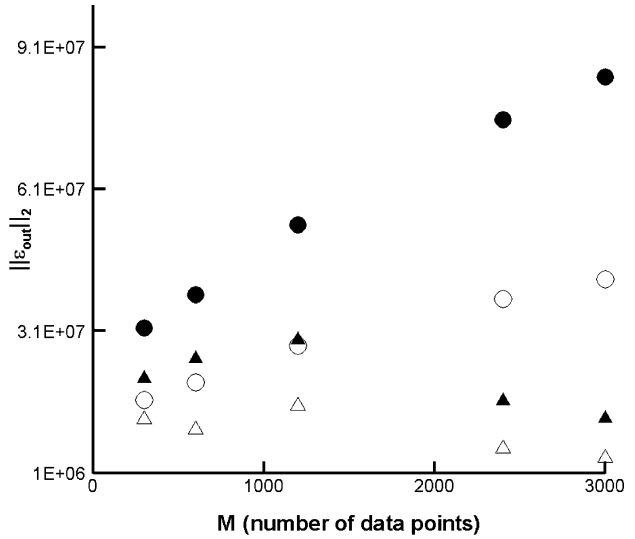

Fig. 7 Rms of the output error, Eq. (9b), when $u = -1$ m/s over sample density (temperature data: ○, $\epsilon_1 = 0.0125$; ●, $\epsilon_1 = 0.025$; and heating/cooling rate data: △, $\epsilon_2 = 0.1$; ▲, $\epsilon_2 = 0.2$).

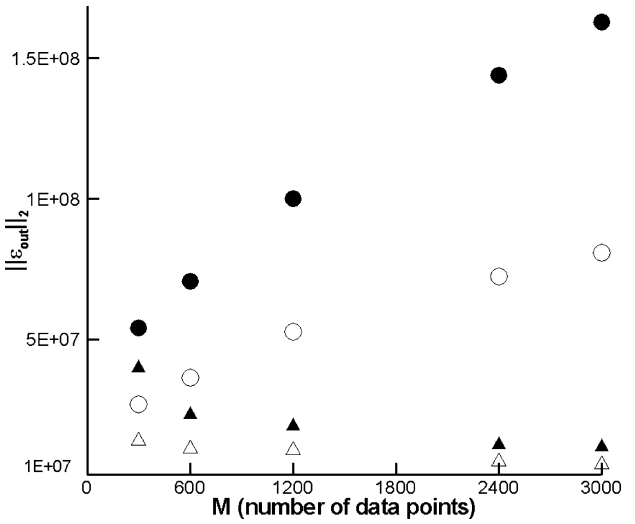

Fig. 8 Rms of the output error, Eq. (9b), when $u = 0$ m/s over sample density (temperature data: ○, $\epsilon_1 = 0.0125$; ●, $\epsilon_1 = 0.025$; and heating/cooling rate data: △, $\epsilon_2 = 0.1$; ▲, $\epsilon_2 = 0.2$).

error as the sample density is increased. This results in an unusable real-time prediction. Figure 6 presents the predicted heat flux using the heating/cooling rate data displayed in Fig. 2. Unlike the temperature data, the heat-flux prediction is accurate in light of the significant amount of input error. Figure 6 portrays error and sampling density trends indicative of a direct problem. In these cases, the numerical integration methods contain enough panels for establishing convergence of the numerical scheme in the presence of ideal discrete data.

Figure 7 displays the behavior of the rms of the output error as the sample density is increased for two induced noise levels for both data types. This plot graphically displays the concept of stability and accuracy based on the data space when $u = -1$ m/s. The rms input error is defined as

$$\|\epsilon_{\mathrm{IN}}(\Psi)\|_2 = \sqrt{\frac{\sum_{i=1}^{M}[\Psi(t_i) - \Psi_i]^2}{M}} \tag{9a}$$

where $\Psi(t)$ is the exact, input data function and Ψ_i is the corresponding discrete, input data with imposed error. Here, $\Psi(t)$ either represents the temperature T_s or heating/cooling rate $\mathrm{d}T_s/\mathrm{d}t$. The rms of the output error is defined as

$$\|\epsilon_{\mathrm{OUT}}(q_s'', \Psi)\|_2 = \sqrt{\frac{\sum_{i=1}^{M}[q_s''(t_i) - q_{s,i}'']^2}{M}} \tag{9b}$$

where $q_{s,i}''$, $i = 1, 2, \ldots, M$ are the numerically obtained values for the heat flux. Equation (9b) also notationally contains the data source used for estimating the heat flux. The rms input data error tends to be relatively constant over M for fixed error ϵ_i, $i = 1, 2$. This is in line with physical expectations associated with random errors and is thus not numerically detailed. Figure 7 displays the rms output error results for $\epsilon_1 = 0.0125$ (open circle), $\epsilon_1 = 0.025$ (filled circle), $\epsilon_2 = 0.1$ (open triangle), and $\epsilon_2 = 0.2$ (filled triangle) as the sample density M is increased. The heating/cooling rate data space clearly presents a favorable trend for the accurate and reliable prediction of the surface heat flux. That is, error reduction is observed when applying heating/cooling rate data while error amplication is observed when applying the temperature data. Again, a significant amount of error is introduced into the heating/cooling rate data to emphasize that these sensors do not require extreme accuracy. The unusual (nonmonotonic) small M behavior for the heating/cooling rate data requires some additional explanation.

Figure 8 presents a similar plot to Fig. 7 but where the front is now assumed stationary (i.e., $u = 0$ m/s). This figure presents a monotonic decay for the rms of the predictive errors based on

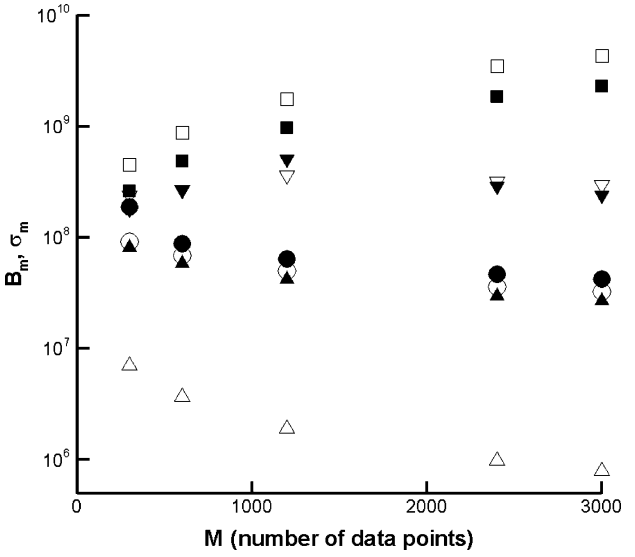

Fig. 9 Deterministic bias B_M (circle, temperature data; triangle, heating/cooling rate data) and variance σ_M (square, temperature data; gradient, heating/cooling rate data) breakdown when $u = 0$ m/s (○, △, □) and $u = -1$ m/s (●, ▲, ■) over sample density (temperature data: $\epsilon_1 = 0.0125$; heating/cooling rate data: $\epsilon_2 = 0.1$).

the heating/cooling rate data. The differential operators (or equivalent integral operators) are different as the convective term vanishes (when $u = 0$ m/s). To clarify this issue further, consideration is directed toward decomposing the predictive heat-flux error into components involving deterministic bias and variance (Ref. 23, p. 180). The difference between the exact heat flux $q_s''(t_i)$ and predictive heat flux in the presence of noisy data $q_{s,i}''$ at time $t = t_i$ is given as

$$q_s''(t_i) - q_{s,i}'' = q_s''(t_i) - q_{s,i,\epsilon=0}'' + q_{s,i,\epsilon=0}'' - q_{s,i}'' \tag{10a}$$

Therefore, one can show

$$\|q_s''(t_i) - q_{s,i}''\|_2 \le B_M + \sigma_M \tag{10b}$$

where the deterministic bias B_M^2 and variance σ_M^2 are defined as

$$B_M^2 = \|q_s''(t_i) - q_{s,i,\epsilon=0}''\|_2^2 \tag{10c}$$

$$\sigma_M^2 = \|q_{s,i,\epsilon=0}'' - q_{s,i}''\|_2^2 \tag{10d}$$

The deterministic bias is a measure involving the ideal discrete data and the exact solution. This indicates the merit of the imposed

numerical method. The variance indicates how sensitive the approach is to random fluctuations in the data. In inverse problems, the bias tends to decrease as the approximation level increases. On the other hand, as the approximation is refined the variance tends to grow. Figure 9 presents results for the square root of the bias B_M and variance σ_M for $u = 0, -1$ m/s when $\epsilon_1 = 0.0125$ and $\epsilon_2 = 0.1$. The simple numerical procedure indicates that the bias decreases as the sample density increases for all four tested cases. The variance caused by the temperature-based data for both velocities tends to grow as the sampling density increases. This is typical of an ill-posed problem [see Eq. (10b)]. In constrast, by changing the data space to involve heating/cooling rate measurements, the variance initially grows and then decreases as the sampling rate increases. This is unlike the behavior of an ill-posed problem. Hence, the highly appealing results shown in Fig. 6 exemplify these remarks.

Conclusions

The purpose of this brief Note is twofold: 1) to derive an inverse-type, moving-boundary-value problem and 2) to demonstrate that it is possible to obtain accurate predictions without difficulty by merely changing the data space.[1] This should assist motivating the development of rate-based thermal sensors for the heat-transfer community especially for applications requiring near, real-time analysis. Future scientific applications could greatly benefit from such a stand-alone sensor solution or integrated into a sensor/analysis simulation. Accurate stand-alone sensors do not guarantee accurate predictions of other quantities unless a clear understanding of how the data space propagates through the mathematical formulation.

References

[1]Frankel, J. I., Osborne, G. E., and Taira, K., "Stabilization of Ill-Posed Problems Through the Data Space," *Journal of Thermophysics and Heat Transfer* (to be published).

[2]Frankel, J. I., and Keyhani, M., "Inverse Heat Conduction: The Need of $\partial T/\partial t$ Data for Design and Diagnostic Purposes," IASTED MIC 99, Paper 113, Calgary, Alberta, Canada, 1999.

[3]Frankel, J. I., and Osborne, G. E., "Motivation for the Development of Heating/Cooling Rate dT/dt and Heat Flux Rate dq''/dt Sensors for Engineering Applications," AIAA Paper 2004-0823, Jan. 2004.

[4]Kulish, V. V., and Novozhilov, V. B., "Integral Equation for the Heat Transfer with the Moving Boundary," *Journal of Thermophysics and Heat Transfer*, Vol. 17, No. 4, 2003, pp. 538–540.

[5]Penner, S. S., and Olfe, D. D., *Radiation and Reentry*, Inst. for Defense Studies, Washington, DC, 1968, Chap. 7.

[6]Kulish, V. V., and Lage, J. L., "Fractional Diffusion Solutions for Transient Local Temperature and Heat Flux," *Journal of Heat Transfer*, Vol. 122, No. 2, 2000, pp. 372–376.

[7]Kulish, V. V., Lage, J. L., Komarov, P. L., and Raad, P. E., "A Fractional-Diffusion Theory for Calculating Thermal Properties of Thin Films from Surface Transient Thermoreflectance Measurements," *Journal of Heat Transfer*, Vol. 123, Dec. 2001, pp. 1133–1138.

[8]Kulish, V. V., and Novozhilov, V. B., "The Relationship Between the Local Temperature and the Local Heat Flux Within a One-Dimensional Semi-Infinite Domain of Heat Wave Propagation," *Mathematical Problems in Engineering*, Hindawi Publ. Corp., Sylvania, OH, 2003 (preprint).

[9]Abramowitz, M., and Stegun, I. A., *Handbook of Mathematical Functions*, Dover, New York, 1972, p. 374.

[10]Lu, F. K., and Kinnear, K. M., "Characterization of Thin Film Heat-Flux Gauges," *20th Advanced Measurement and Ground Testing Technology Conference*, AIAA, Reston, VA, 1998, pp. 98–2504.

[11]Cook, W. J., and Felderman, E. J., "Reduction of Data from Thin-Film Heat Transfer Gages: A Concise Numerical Technique," *AIAA Journal*, Vol. 4, No. 3, 1966, pp. 561, 562.

[12]Cook, W. J., "Determination of Heat Transfer Rates from Transient Surface Temperature Measurements," *AIAA Journal*, Vol. 8, No. 7, 1970, pp. 1366–1368.

[13]Bocher, M., *An Introduction to the Study of Integral Equations*, Cambridge Univ. Press, Cambridge, England, U.K., 1926, Chaps. 2, 3.

[14]Linz, P., *Analytical and Numerical Methods for Volterra Equations*, Society for Industrial and Applied Mathematics, Philadelphia, PA, 1985, Chap. 5.

[15]Baker, C. T. H., *The Numerical Treatment of Integral Equations*, Clarendon Press, Oxford, England, U.K., 1978, Chap. 6.

[16]Golberg, M. A. (ed.), *Solution Methods for Integral Equations*, Plenum, New York, 1979, Chap. 1.

[17]Kaplan, W., *Advanced Calculus*, 2nd ed., Addison Wesley Longman, Reading, MA, 1973, p. 287.

[18]Kress, R., *Linear Integral Equations*, Springer-Verlag, Berlin, 1989, Chap. 15.

[19]Wing, G. M., *A Primer on Integral Equations of the First Kind*, Society for Industrial and Applied Mathematics, Philadelphia, PA, 1991, Chap. 2.

[20]Hanke, M., and Scherzer, O., "Inverse Problems Light: Numerical Differentiation," *American Mathematical Monthly*, Vol. 108, June/July 2001, pp. 512–520.

[21]Groetsch, T., "Differentiation of Approximately Specified Functions," *American Mathematical Monthly*, Vol. 98, No. 9, 1991, pp. 847–850.

[22]Frankel, J. I., Keyhani, M., and Taira, K., "In-Phase Error Estimation of Experimental Data and Optimal First Derivatives," *AIAA Journal*, Vol. 42, No. 5, 2004, pp. 1017–1024.

[23]Kurpisz, K., and Nowak, A. J., *Inverse Thermal Problems*, Computational Mechanics Publishing, Southampton, England, U.K., 1995, p. 180.